LETTER

doi:10.1038/nature14502

Experimental constraints on the electrical anisotropy of the lithosphere–asthenosphere system

Anne Pommier[1,2], Kurt Leinenweber[3], David L. Kohlstedt[4], Chao Qi[4], Edward J. Garnero[2], Stephen J. Mackwell[5] & James A. Tyburczy[2]

The relative motion of lithospheric plates and underlying mantle produces localized deformation near the lithosphere–asthenosphere boundary[1]. The transition from rheologically stronger lithosphere to weaker asthenosphere may result from a small amount of melt or water in the asthenosphere, reducing viscosity[1–3]. Either possibility may explain the seismic and electrical anomalies that extend to a depth of about 200 kilometres[4,5]. However, the effect of melt on the physical properties of deformed materials at upper-mantle conditions remains poorly constrained[6]. Here we present electrical anisotropy measurements at high temperatures and quasi-hydrostatic pressures of about three gigapascals on previously deformed olivine aggregates and sheared partially molten rocks. For all samples, electrical conductivity is highest when parallel to the direction of prior deformation. The conductivity of highly sheared olivine samples is ten times greater in the shear direction than for undeformed samples. At temperatures above 900 degrees Celsius, a deformed solid matrix with nearly isotropic melt distribution has an electrical anisotropy factor less than five. To obtain higher electrical anisotropy (up to a factor of 100), we propose an experimentally based model in which layers of sheared olivine are alternated with layers of sheared olivine plus MORB or of pure melt. Conductivities are up to 100 times greater in the shear direction than when perpendicular to the shear direction and reproduce stress-driven alignment of the melt. Our experimental results and the model reproduce mantle conductivity–depth profiles for melt-bearing geological contexts. The field data are best fitted by an electrically anisotropic asthenosphere overlain by an isotropic, high-conductivity lowermost lithosphere. The high conductivity could arise from partial melting associated with localized deformation resulting from differential plate velocities relative to the mantle, with subsequent upward melt percolation from the asthenosphere.

Electromagnetic profiles of the lithosphere–asthenosphere system reveal zones of high electrical conductivity and electrical anisotropy, which vary with depth (Fig. 1)[5,7,8]. High conductivity can be attributed to several factors, including the presence of an interconnected fluid phase[9]. Regions of electrical anisotropy are usually attributed to mantle deformation that can result from the motion of rigid lithospheric plates relative to the underlying convecting mantle[3,4]. Experimental investigations under controlled laboratory conditions allow a direct assessment of the effect of deformation and chemistry on electrical conductivity, an important step in investigating the dynamic coupling of tectonic plates with the underlying mantle.

The current laboratory-derived database of electrical anisotropy of mantle materials consists principally of measurements of electrical conductivity σ for different crystallographic orientations of dry and hydrous olivine single crystals[10,11]. Only one set of measurements has been made for σ of melt-bearing olivine aggregates during torsion[12], and these experiments were performed at low crustal pressure (0.3 GPa) and only to low shear strain ($\gamma < 0.5$–1), limiting the formation of noticeable melt bands. Recently, new electrical measurements on melt + olivine aggregates were performed during simple shear at 3 GPa, but only small strains ($\gamma < 1.8$) were reached[13].

Here we report the results of laboratory experiments at asthenospheric pressure (about 3 GPa) and on samples previously deformed to high strains ($\gamma \approx 9$). These experiments were designed to investigate electrical anisotropy in deformed mantle materials, in order to develop an electrical model of the upper mantle to be compared with field results. The electrical anisotropy of mantle materials was investigated by measuring the electrical conductivity of previously deformed sam-

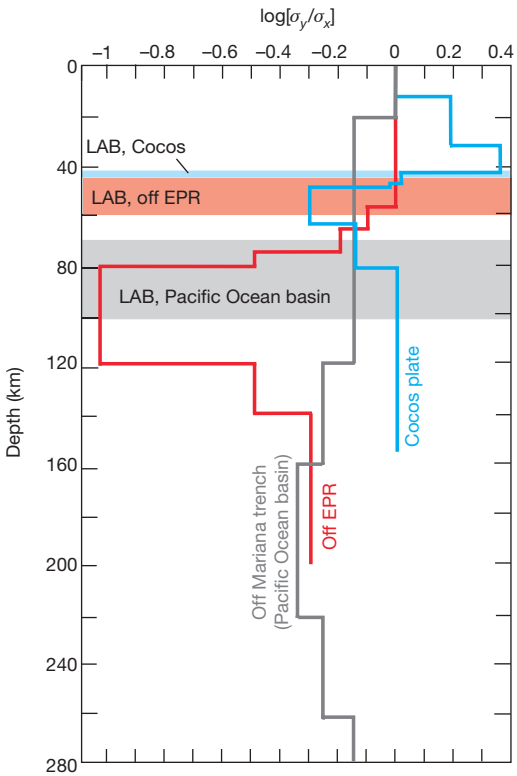

Figure 1 | Anisotropic conductivity models obtained from inversion of electromagnetic data in different geological contexts. The conductivity ratio is for perpendicular directions σ_y and σ_x, with σ_x the direction of highest conductivity in the asthenosphere. Electrical profiles are for the Pacific Ocean Basin (off the Mariana Trench) in grey, the East Pacific Rise (EPR, 200 km off the ridge axis) in red, and the Cocos plate (250 km off trench) in blue[5,7,8]. Anisotropy in the lithosphere under the Cocos plate is not well constrained. All profiles present a sublithospheric or asthenospheric region of high anisotropy, topped with a low-anisotropy layer.

[1]University of California San Diego, Scripps Institution of Oceanography, Institute of Geophysics and Planetary Physics, La Jolla, California 92093, USA. [2]School of Earth and Space Exploration, Arizona State University, Tempe, Arizona 85287, USA. [3]Department of Chemistry and Biochemistry, Arizona State University, Tempe, Arizona 85287, USA. [4]Department of Earth Sciences, University of Minnesota, Minneapolis, Minnesota 55455, USA. [5]Lunar and Planetary Institute, Universities Space Research Association, Houston, Texas 77058, USA.

ples in a multi-anvil apparatus at about 3 GPa and up to 1,300 °C in two perpendicular directions using impedance spectroscopy (Extended Data Fig. 1).

Dry polycrystalline olivine samples (Fo_{90}), a Fo_{90} + 5 vol% MORB sample, and a Fo_{90} + 2 vol% $NaKCO_3$ melt sample were used. These samples were initially deformed in triaxial compression or in simple shear (Methods and Extended Data Table 1) at a confining pressure P = 0.3 GPa and a temperature T = 1,200–1,250 °C in a gas-medium apparatus. The parts of the samples that had experienced maximum shear strain were extracted and placed in a conductivity cell in the multi-anvil apparatus (Extended Data Table 1) for measurements of electrical properties at a pressure representative of the pressure of the asthenosphere.

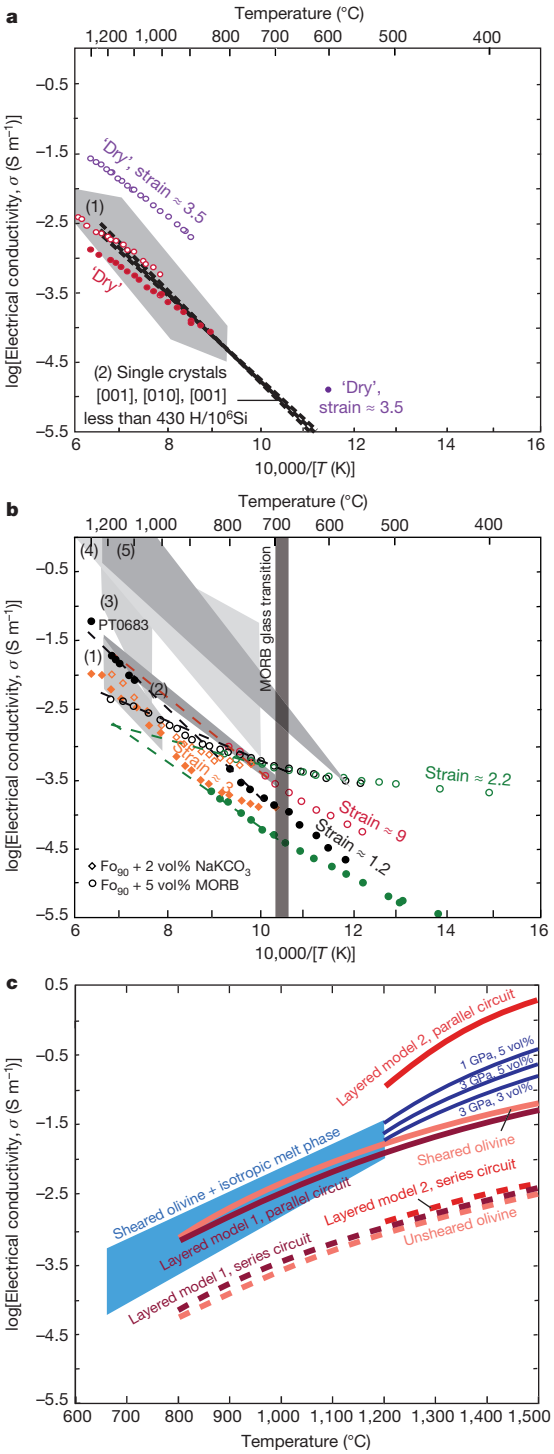

Measurements were primarily conducted under quasi-hydrostatic conditions at temperatures not exceeding 900 °C with a few experiments at temperatures near 1,300 °C (Methods). In the low-temperature conductivity runs, melt-enriched sheets (bands in two dimensions) formed during deformation runs are preserved as previously observed[14,15], whereas after the high-temperature conductivity experiments the melt-rich bands are no longer detected (Extended Data Fig. 2). Instead, melt-bearing samples quenched from high-temperature measurements (>~1,100 °C) exhibited a sheared solid matrix with an approximately homogeneous (meaning a lack of melt-rich bands) and isotropic melt distribution, because in the high-temperature conductivity experiments, surface tension relatively quickly redistributes the melt, both in terms of dissipation of the melt-rich bands and in terms of randomization of the orientation of melt-filled triple junctions, thus removing the melt preferred orientation introduced by deformation[16,17].

Nonetheless, a small degree of heterogeneity in melt distribution remained, with some areas showing slightly higher melt concentrations than others. This observation suggests that some structural anisotropy associated with the deformation-induced lattice preferred orientation persists for the duration of our conductivity measurements, in agreement with previous observations on sheared samples that were statically annealed after large strain deformation[18]. Chemical analyses of run products are consistent with starting compositions (Extended Data Table 2).

Because the temperature of the lithosphere–asthenosphere system is not well constrained, our experiments investigated the electrical properties of mantle analogues over a wide range of temperature. For olivine samples, a single Arrhenius relationship can satisfactorily reproduce the electrical data over the investigated temperature range (Fig. 2a; Extended Data Table 3). For both MORB-bearing and carbonate-bearing samples, a slight bowing in the trend of electrical conductivity with temperature is observed at about 870–900 °C, possibly caused by textural changes. Electrical data are therefore best reproduced by two Arrhenius equations, one on either side of this temperature (Fig. 2b; Extended Data Table 4). For experiments performed at low temperature (<900 °C) on melt-bearing samples, values of σ at

Figure 2 | Electrical conductivity–temperature diagrams of experimental results. a, Results for olivine aggregates at low and high shear strains. Open and closed circles represent data parallel to and perpendicular to the main deformation direction, respectively. Our data agree well with grey zone (1), which corresponds to σ of olivine aggregates under pressure[26,27]. Electrical data on olivine single crystal in different crystallographic directions (zone (2), with water content less than 430 H atoms per 10^6 Si atoms) are from ref. 10. **b**, Results for the melt-bearing systems. Open and closed symbols represent data parallel to and perpendicular to the main deformation direction, respectively. Only the electrical measurements of carbonate-bearing samples (diamonds) and of the MORB-bearing sample with a strain of 1.2 in the direction parallel to the main deformation (open black circles) were performed over a large temperature range from high to low temperature. All other experiments were performed either at high (>1,100 °C) or at low (<900 °C) temperature (Extended Data Table 4). Good agreement is obtained with data from zone (1)[12]. The slight difference in the results from zone (2) at 0.1 MPa (ref. 28) is consistent with the effect of pressure. The conductivities from refs 29 and 30 (zones (3), (4), and (5)) are higher than the ones measured in this study, possibly owing to melt chemistry effects. The dashed lines are Arrhenius relations for conductivity in the post-glass transition temperature range. Electrical anisotropy decreases with increasing temperature to become negligible at high temperature. **c**, Laboratory-based isotropic (blue colours) and anisotropic (red colours) models of the electrical conductivity of deformed mantle materials. Models are based on Arrhenius equations and on extrapolations of our results from low- to high-temperature experiments. Isotropic models for MORB-bearing samples at >1,200 °C are based on the Hashin–Shtrikman upper bound. Layered model 1 considers layers of polycrystalline olivine alternating with layers of sheared Fo_{90} + 5 vol% MORB, and layered model 2 considers layers of polycrystalline olivine alternating with layers of basalt[22] (see Methods).

higher T can be calculated by extrapolating electrical data collected above the glass transition (at about 670 °C) (dashed lines in Fig. 2b; Extended Data Table 4). Although this extrapolation to high temperature does not account for the slight bowing in the slope observed at around 870–900 °C for high-temperature samples, it provides a constraint with the least amount of uncertainty on conductivity–strain relationships because the melt phase did not redistribute in these low-temperature experiments. It also satisfactorily reproduces the measurements of high-temperature samples performed up to 1,300 °C (sample PT0683, Fig. 2b). In fact, the electrical conductivity of melts with a low degree of polymerization shows no major change in activation energy at temperatures above the glass transition temperature to 1,300 °C (ref. 19), and previous experimental studies have demonstrated that a single activation energy describes the electrical conductivity of olivine over the temperature range of interest, 700–1,300 °C (ref. 20).

Our results, which quantify the effects of deformation and partial melt on the electrical conductivity of mantle rocks, are summarized as follows. (1) Deformation affects the electrical response of all the systems investigated, including both melt-free olivine compacts and melt + olivine samples (Fig. 2). This observation contrasts with results from a previous study[13] that did not show anisotropy in sheared melt-free samples, possibly because the shear strains were too low ($\gamma < 1.8$). The effect on conductivity anisotropy of a relatively small amount of strain in triaxial compression of olivine aggregates is small (a factor of <2) but detectable (Fig. 2a). Simple shear deformation in torsion of olivine aggregates to a relatively large shear strain ($\gamma \approx 3.5$) results in an enhancement by a factor of about ten in electrical conductivity parallel to the direction of shear compared to an undeformed sample. For this sample (PT0264), the lattice preferred orientation of olivine is defined by [100] subparallel to the shear direction, and by (010) subparallel to the shear plane (also called type-A fabric)[21]. The lattice preferred orientation of the olivine grains is unlikely to explain the high bulk conductivity of this sheared sample, because electrical anisotropy in olivine single crystals is only about a factor of two at 1,200 °C (ref. 10), much smaller than our measured factor of ten. The high conductivity in the high-strain sample may be due to the contribution of grain boundaries, as the grain size in the sheared samples is smaller than in an undeformed sample owing to dynamic recrystallization and the grain boundaries are sympathetically oriented in the shear samples. The decrease in activation energy observed for most samples at high temperature (more than about 1,040 °C) may be an indication that the stress regime preserved from the deformation experiment has relaxed to a greater degree during the electrical experiment. However, the deformed texture of the sample was preserved during the entire experiment (Extended Data Fig. 2a). No systematic effect of shear strain (for $1.2 < \gamma < 9$) on conductivity was observed for melt-bearing samples (Fig. 2b).

(2) The addition of a few volume per cent of basaltic or carbonate melt to a polycrystalline olivine slightly increases the bulk electrical conductivity (by 10%–30%). For all melt-bearing samples, electrical anisotropy is large at low T in the glass region and above the glass transition temperature T_g up to 900 °C, but decreases at temperatures greater than 900 °C, consistent with the disappearance of melt-rich bands in the run products during the high-temperature conductivity experiments (Extended Data Fig. 2). This low electrical anisotropy at high temperature indicates a reorganization of the melt network in the multi-anvil apparatus, despite the persistence of some degree of structural anisotropy: the crystallographic preferred orientation of the olivine grains was maintained, but the melt preferred orientation weakened (controlled by anisotropy in the melt–solid interfacial energy rather than by stress) and the melt-rich bands dissipated in response to surface tension, leaving a nearly isotropic melt distribution. Samples with 5 vol% MORB and 2 vol% carbonate yield similar values for conductivity at a given temperature. From their electrical response alone, all investigated materials can potentially explain high conductivities in the upper mantle (typically ≥ 0.03 S m^{-1}), emphasizing that electrical conductivity alone cannot discriminate between the effect of bulk composition and deformation textures.

On the basis of the results of our experiments, we propose models for the electrical conductivity in both anisotropic and predominantly isotropic environments (Fig. 2c). Melt-bearing samples provide analogues of a melt-bearing isotropic mantle and of melt-rich bands in a highly anisotropic mantle. The bulk electrical conductivity of a banded mantle is calculated using a layered model that consists of either series or parallel circuit equations, depending on the direction considered (Methods). In this model, melt-rich layers correspond to either a MORB-bearing material using our conductivity measurements or a basaltic material

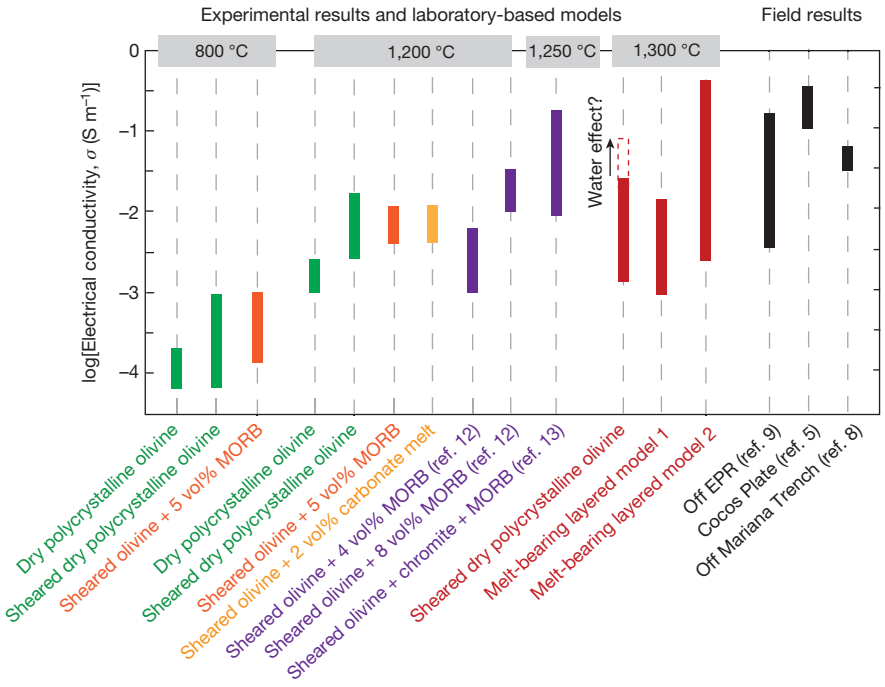

Figure 3 | Comparison between the electrical anisotropy of deformed materials measured in laboratory experiments and that determined from field measurements. Experimental results are from this study and refs 12 and 13, and field results are the same as in Fig. 1[5,7,8]. Calculations using the laboratory-based layered model are explained in Methods. Large anisotropies are well reproduced with the layered model and sheared olivine. The addition of water may increase the electrical anisotropy of sheared olivine. High temperatures are needed to match the highest conductivity values ($\sigma > 0.1$ S m^{-1}) observed in the field. Electrical results at 800 °C are not shown for the carbonate-bearing material because this sample was first taken to high temperature (before being cooled down), where the melt homogenized and damaged the anisotropic texture.

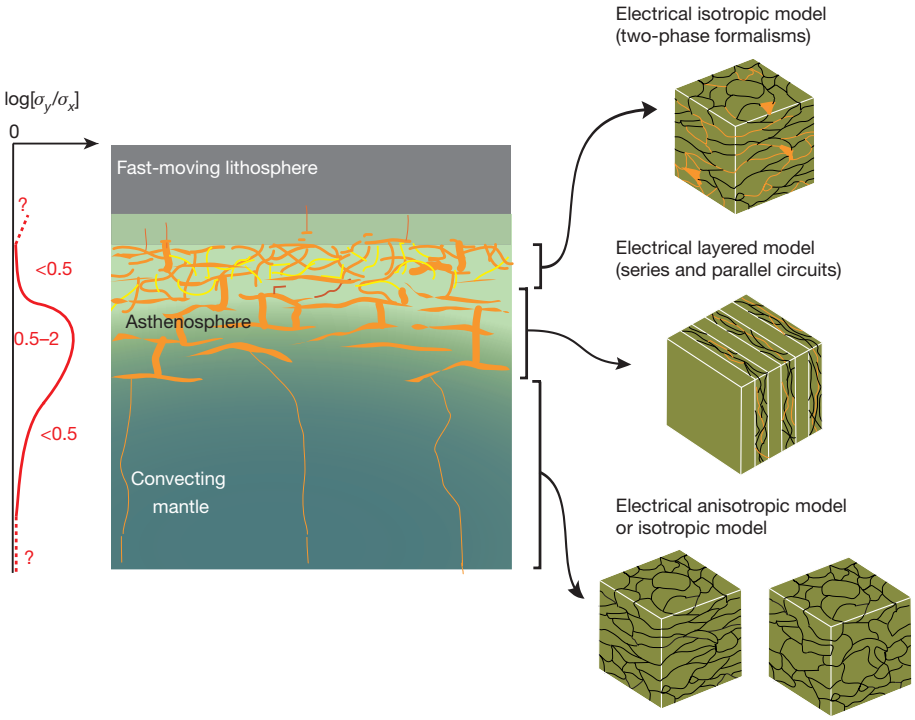

Figure 4 | Cross-section portrayal of the electrical conductivity of the uppermost mantle in a melt-bearing context. The corresponding conductivity ratio for the direction of lowest (σ_y) to the highest (σ_x) conductivity is shown in red. Melt reaches the asthenosphere from the deeper mantle. The geometry and the distribution of melt pathways in the deeper mantle do not significantly affect electrical anisotropy. In the asthenosphere, the horizontal alignment (of sheets, tubules, and so on) is the dominant process and results from mantle flow so electrical anisotropy is enhanced as a result of plate motion. Vertical melt migration has an insignificant influence on the geophysical response. Melt accumulates at the bottom of the lithosphere because the lithosphere is less permeable, and becomes well interconnected in all directions despite a deformed solid matrix. This melt is isolated from mantle flow, cooling and crystallizing.

based on published conductivity results[22]; melt-free layers correspond to either undeformed or sheared polycrystalline Fo_{90}.

Our results reproduce both the magnitude and the anisotropy of electrical conductivity in various melt-bearing contexts (Fig. 3). Near the East Pacific Rise, where a few volume per cent of melt is expected, the high anisotropy ($\sigma_{max}/\sigma_{min} > 50$, Fig. 3) detected at a depth of 80–120 km is best reproduced by a laboratory-based layered model (melt-bearing layered model 2 in Fig. 3) that is consistent with plate-motion-related strains in the asthenosphere that induce alignment of melt and formation of melt-enriched sheets in the direction of plate motion.

Under the Cocos plate, the main conductivity anomaly in the asthenosphere (45–60 km) has a small anisotropy ($\sigma_{max}/\sigma_{min} \approx 3$, Fig. 3) despite the fact that the high speed of the plate (8.5 cm yr^{-1}) is expected to be accompanied by substantial strain in the underlying asthenosphere. Our layered models are too anisotropic to be comparable to field observations under the Cocos plate (Fig. 3), suggesting that the geometric configuration of the melt phase under the Cocos plate is almost electrically isotropic. In highly deformed rocks, a low degree of anisotropy of the melt phase may appear paradoxical. However, this possibility can be reconciled at high temperatures, where stresses are lower and thus deformation produces a weaker crystallographic preferred orientation and melt preferred orientation than at lower T where stress is higher (to maintain the same strain rate). Temperatures exceeding 1,400 °C with a few volume per cent of hydrous melt have been previously suggested to explain these high conductivities[5]. Our experiments demonstrate that a temperature of around 1,300 °C is sufficient to explain the observed conductivities and that the weak anisotropy is reproduced by a sheared material in which melt pathways exist in all directions.

Under the Pacific Ocean basin, at more than 100 km east of the Mariana Trench and at a depth of 150–250 km, the weak electrical anisotropy ($\sigma_{max}/\sigma_{min} \approx 1.8$, Fig. 3) has been attributed to mantle flow in the Mariana Trough[7]. As for the Cocos plate, the field data are best reproduced by an isotropic melt phase interconnected in a sheared solid matrix at high temperature (>1,200 °C). The extrapolation of Arrhenian equations based on our data on sheared olivine + 5 vol% MORB (Fig. 2b; Extended Data Table 4) to 1,350 °C reproduces the electrical field data off the Mariana Trench, with electrical conductivity values of 6.4×10^{-2} S m^{-1} in the direction of deformation and 2.7×10^{-2} S m^{-1} in the direction perpendicular to deformation.

Regions of high anisotropy embedded between layers of low anisotropy that have been observed beneath mid-ocean ridges and oceanic plates (Fig. 1) can be related to vertical stratification in mantle rheology and fluid distribution (Fig. 4). Deep regions of low anisotropy are observed under the East Pacific Rise, the Cocos plate, and the Pacific Ocean basin (at depths of 140 km, 80 km and 250 km, respectively), consistent with an isotropic distribution of mantle phases and possibly scattered melt pathways towards shallower asthenospheric depths. At shallower depths, the decrease in electrical anisotropy and conductivity observed for the regions considered (less than about 80 km depth off the East Pacific Rise, 40–45 km depth under the Cocos plate, and less than about 120 km depth off the Mariana Trench, Fig. 1) may involve processes associated with the coupling of tectonic plate motion and flow in the underlying mantle. Layers of low electrical anisotropy are consistent with a more isotropically distributed melt phase that governs the bulk conductivity. An interconnected liquid phase with a weak melt preferred orientation in a deformed matrix may also explain why some electromagnetic studies in other locations observe high conductivities but do not detect electrical anisotropy[23]. This melt distribution may arise from its accumulation at the lithosphere–asthenosphere boundary and possible upward migration through dikes that propagate buoyantly into the lithosphere[24,25]. It is also possible that asthenospheric melt percolates into the bottom of the lithosphere, eventually cooling and crystallizing. If the long-term rheological behaviour of crystallizing melt-rich structures results in increasing the viscosity in a zone at the base of the lithosphere, it can then reduce the efficiency of viscous coupling between the tectonic plates and the underlying flow of the mantle through time.

Online Content Methods, along with any additional Extended Data display items and Source Data, are available in the online version of the paper; references unique to these sections appear only in the online paper.

Received 16 June 2014; accepted 21 April 2015.

1. Holtzman, B. K. & Kendall, J.-M. Organized melt, seismic anisotropy, and plate boundary lubrication. *Geochem. Geophys. Geosyst.* **11,** Q0AB06 (2010).

2. Höink, T., Lenardic, A. & Richards, M. Depth-dependent viscosity and mantle stress amplification: implications for the role of the asthenosphere in maintaining plate tectonics. *Geophys. J. Int.* **191,** 30–41 (2012).
3. Karato, S.-i. On the origin of the asthenosphere. *Earth Planet. Sci. Lett.* **321–322,** 95–103 (2012).
4. Kawakatsu, H. *et al.* Seismic evidence for sharp lithosphere-asthenosphere boundaries of oceanic plates. *Science* **324,** 499–502 (2009).
5. Naif, S., Key, K., Constable, S. & Evans, R. L. Melt-rich channel observed at the lithosphere–asthenosphere boundary. *Nature* **495,** 356–359 (2013).
6. Hirschmann, M. M. Partial melt in the oceanic low velocity zone. *Phys. Earth Planet. Inter.* **179,** 60–71 (2010).
7. Matsuno, T. *et al.* Upper mantle electrical resistivity structure beneath the central Mariana subduction system. *Geochem. Geophys. Geosyst.* **11,** Q09003 (2010).
8. Baba, K., Chave, A. D., Evans, R. L., Hirth, G. & Mackie, R. L. Mantle dynamics beneath the East Pacific Rise at 17 °S: insights from the Mantle Electromagnetic and Tomography (MELT) experiment. *J. Geophys. Res.* **111,** B02101 (2006).
9. Reynard, B., Mibe, K. & Van de Moortèle, B. Electrical conductivity of the serpentinised mantle and fluid flow in subduction zones. *Earth Planet. Sci. Lett.* **307,** 387–394 (2011).
10. Yoshino, T., Takuya, M., Yamashita, S. & Katsura, T. Hydrous olivine unable to account for conductivity anomaly at the top of the asthenosphere. *Nature* **443,** 973–976 (2006).
11. Poe, B. T., Romano, C., Nestola, F. & Smyth, J. R. Electrical conductivity anisotropy of dry and hydrous olivine at 8 GPa. *Phys. Earth Planet. Inter.* **181,** 103–111 (2010).
12. Caricchi, L., Gaillard, F., Mecklenburgh, J. & Le Trong, E. Experimental determination of electrical conductivity during deformation of melt-bearing olivine aggregates: implications for electrical anisotropy in the oceanic low velocity zone. *Earth Planet. Sci. Lett.* **302,** 81–94 (2011).
13. Zhang, B., Yoshino, T., Yamazaki, D., Manthilake, G. & Katsura, T. Electrical conductivity anisotropy in partially molten peridotite under shear deformation. *Earth Planet. Sci. Lett.* **405,** 98–109 (2014).
14. Holtzman, B. K. *et al.* Melt segregation and strain partitioning: implications for seismic anisotropy and mantle flow. *Science* **301,** 1227–1230 (2003).
15. King, D. S., Kohlstedt, D. L. & Zimmerman, M. E. Stress-driven melt segregation in partially molten rocks deformed in torsion. *J. Petrol.* **51,** 21–42 (2010).
16. Parsons, R. A., Nimmo, F., Hustoft, J., Holtzman, B. K. & Kohlstedt, D. L. An experimental and numerical study of surface tension-driven melt flow. *Earth Planet. Sci. Lett.* **267,** 548–557 (2008).
17. King, D. S. H., Hier-Majumder, S. & Kohlstedt, D. L. An experimental study of the effects of surface tension in homogenizing perturbations in melt fraction. *Earth Planet. Sci. Lett.* **307,** 349–360 (2011).
18. Kohlstedt, D. L. & Zimmerman, M. E. Rheology of partially molten mantle rocks. *Annu. Rev. Earth Planet. Sci.* **24,** 41–62 (1996).
19. Pommier, A., Gaillard, F., Pichavant, M. & Scaillet, B. Laboratory measurements of electrical conductivities of hydrous and dry Mount Vesuvius melts under pressure. *J. Geophys. Res.* **113,** B05205 (2008).
20. Constable, S. SEO3: a new model of olivine electrical conductivity. *Geophys. J. Int.* **166,** 435–437 (2006).
21. Jung, H., Katayama, I., Jiang, Z., Hiraga, T. & Karato, S. Effect of water and stress on the lattice-preferred orientation of olivine. *Tectonophysics* **421,** 1–22 (2006).
22. Ni, H., Keppler, H. & Behrens, H. Electrical conductivity of hydrous basaltic melts: implications for partial melting in the upper mantle. *Contrib. Mineral. Petrol.* **162,** 637–650 (2011).
23. Evans, R. L., Wannamaker, P. E., McGary, R. S. & Elsenbeck, J. Electrical structure of the central Cascadia subduction zone: the EMSLAB Lincoln Line revisited. *Earth Planet. Sci. Lett.* **402,** 265–274 (2014).
24. Havlin, C., Parmentier, E. M. & Hirth, G. Dike propagation driven by melt accumulation at the lithosphere–asthenosphere boundary. *Earth Planet. Sci. Lett.* **376,** 20–28 (2013).
25. Sakamaki, T. *et al.* Ponded melt at the boundary between the lithosphere and asthenosphere. *Nature Geosci.* **6,** 1041–1044 (2013).
26. Dai, L., Li, H., Li, C., Hu, H. & Shan, S. The electrical conductivity of dry polycrystalline olivine compacts at high temperatures and pressures. *Mineral. Mag.* **74,** 849–857 (2010).
27. Xu, Y. S., Shankland, T. J. & Duba, A. G. Pressure effect on electrical conductivity of mantle olivine. *Phys. Earth Planet. Inter.* **118,** 149–161 (2000).
28. Roberts, J. J. & Tyburczy, J. A. Partial-melt electrical conductivity: influence of melt composition. *J. Geophys. Res.* **104,** 7055–7065 (1999).
29. Yoshino, T., Laumonier, M., McIsaac, E. & Katsura, T. Electrical conductivity of basaltic and carbonatite melt-bearing peridotites at high pressures: implications for melt distribution and melt fraction in the upper mantle. *Earth Planet. Sci. Lett.* **295,** 593–602 (2010).
30. Yoshino, T., McIsaac, E., Laumonier, M. & Katsura, T. Electrical conductivity of partial molten carbonate peridotite. *Earth Planet. Sci. Lett.* **194–195,** 1–9 (2012).

Acknowledgements This work benefited from funding by the NSF through Cooperative Studies of the Earth's Deep Interior (CSEDI) projects number 1461594 to the University of California San Diego, number 1265395 to Arizona State University, and number 1265428 to the University of Minnesota. This research was partially supported by COMPRES (the Consortium for Materials Properties Research in Earth Sciences) under National Science Foundation (NSF) Cooperative Agreement EAR 11-57758 (cell assembly development project). We thank A. von der Handt (University of Minnesota) and H. Cathey (Arizona State University) for their assistance with the electron microprobe and scanning electron microscope imaging, respectively. A.P. appreciates help with calibration experiments from staff and scientists at Bayerisches GeoInstitut (BGI). This paper is Lunar and Planetary Institute (LPI) contribution number 1840.

Author Contributions A.P. proposed and led the project, performed the conductivity experiments and the electron microprobe analyses, interpreted the results, wrote the first draft and made the figures. K.L. and A.P. developed the conductivity setup at Arizona State University. D.L.K. and C.Q. synthesized the deformed starting materials and provided some of the scanning electron microscope images. E.J.G., S.J.M. and D.L.K. contributed to the data interpretation and discussion. All authors commented on the manuscript and provided editorial assistance.

Author Information Reprints and permissions information is available at www.nature.com/reprints. The authors declare no competing financial interests. Readers are welcome to comment on the online version of the paper. Correspondence and requests for materials should be addressed to A.P. (pommier@ucsd.edu).

METHODS

Starting materials. Electrical measurements were performed on three anhydrous starting materials: polycrystalline olivine (Fo_{90}), Fo_{90} + 5 vol.% MORB, and Fo_{90} + 2 vol.% $NaKCO_3$ melt. These samples were deformed in triaxial compression to a strain of approximately 0.1 or in simple shear to shear strains from 1.2 to 9 (Extended Data Table 1) at a confining pressure of 0.3 GPa and temperatures of 1,200 °C–1,250 °C in a gas-medium apparatus. The parts of the samples that had experienced maximum shear strain were extracted and placed in a conductivity cell in the multi-anvil apparatus (Extended Data Fig. 1a) for electrical measurements. Simultaneous monitoring of the deformation and the electrical response is not required to investigate the effect of deformation on the electrical conductivity and anisotropy in σ of polycrystalline materials, as long as the same starting material is used to do the measurements in the different orientations. Note that the gas-medium apparatus used to deform the samples is operated at low pressure (0.3 GPa), whereas the multi-anvil apparatus can reproduce asthenospheric conditions (in our case, about 3 GPa).

Multi-anvil experiments. All electrical experiments were performed at about 3 GPa in a multi-anvil apparatus using tungsten carbide cubes with a corner-truncation edge length of 8 mm and mullite octahedral pressure media with an edge length of 14 mm. Graphite heaters were used, placed inside an outer zirconia sleeve that provided thermal insulation. Experimental samples were 2 mm in diameter and 0.8–1.5 mm in length, and were placed at the centre of the cylindrical heater inside an MgO sleeve. Two molybdenum disks (outer diameter 2 mm) were in contact with the sample, serving as electrodes. The temperature was monitored with a $W_{95}Re_5$–$W_{74}Re_{26}$ (C-type) thermocouple inserted within an MgO sleeve with the junction in contact with the top of one of the molybdenum disks (Extended Data Fig. 1b). A single tungsten–rhenium (W–Re) wire was connected to the other molybdenum disk.

The conductivity cell (Extended Data Fig. 1b) was connected to a 1260 Solartron Impedance/Gain-Phase Analyzer for electrical impedance measurements. Redox conditions (oxygen fugacity) were not controlled during the experiments. However, the presence of a graphite furnace implies a reducing environment with an oxygen fugacity near the fayalite–magnetite–quartz buffer[31].

To preserve the influence of deformation and chemistry on conductivity, heating duration in the multi-anvil conductivity experiments did not exceed 2 h, and measurements were preferentially conducted at temperatures <900 °C. As illustrated by Extended Data Fig. 2c and f, melt-rich bands were preserved at temperatures slightly above the glass transition. This observation is consistent with previous experimental work on sheared melt-bearing materials, which demonstrated that annealing at about 1,100 °C and below causes essentially no melt redistribution over laboratory timescales[16,32].

Electrical conductivity cell calibration. Our electrical cell has been tested using a hot-pressed polycrystalline olivine sample (wet Fo_{75}) by performing σ experiments under the same conditions (same sample, pressure and temperature) in two different laboratories (Arizona State University and Bayerisches GeoInstitut). The cell used at BGI was different from the one used at ASU, in terms of both materials and part dimensions. Electrical conductivity data were collected at 3 GPa and at temperatures up to 700 °C. All data from both laboratories fitted into a 3% error in logσ, confirming that our cell was measuring the sample's response without interference from any other part of the cell assembly. A short-circuit experiment performed at 4 GPa and at temperature up to 1,900 °C showed that our cell has a resistance of about 7 Ω (ref. 33), which is negligible compared to the resistance of our samples (>3,000 Ω).

Electrical conductivity measurements. The complex impedance was collected during cooling over different temperature ranges (Extended Data Tables 3 and 4) in the frequency range 1 Hz to 5 MHz. The reproducibility of electrical measurements was validated by performing a few measurements during heating. For melt-free samples and melt-bearing samples at low temperature, the electrical response consisted of an impedance arc (Extended Data Fig. 1c). For MORB-bearing samples at high temperature, the impedance arc was not observed and the electrical response consisted of a noisy part at high frequency and a vertical line at low frequency intersecting with the real axis of the complex plane. For all samples, the electrical resistance of the sample corresponds to the real part of the complex impedance, identified in the real versus imaginary component plot as the intercept of the spectrum with the real axis.

Data reduction and uncertainties. For each sample, the electrical conductivity was calculated using the measured electrical resistance and sample geometric factor G (ref. 34)

$$\sigma = 1/(RG) \quad (1)$$

where $G = \pi r^2/L$, σ is the electrical conductivity (in units of S m−1), R is the electrical resistance (in ohms), r is the radius of the cylindrical sample (in metres), and L is the thickness of the sample (in metres). Relative errors on values of σ (Extended Data Tables 3 and 4) were calculated on the basis of errors on the geometrical factor (that is, considering errors on r and L) as well as propagated errors on each measured value of resistance R. As an example, uncertainties on electrical conductivity values are provided in Extended Data Table 5 for each temperature of the experiment on sample PT0683-2.

Analytical techniques. All the recovered run products were mounted in epoxy resin and then ground and polished (using ethanol for the carbonate-bearing samples to preserve the carbonate phase, and using water for all the other samples) for analytical investigations. Scanning electron microscope imaging and electron microprobe analyses were performed after each experiment to characterize the texture and chemistry of the samples. The chemical compositions of melt and mineral phases were obtained using a JEOL JXA-8900 Electron Probe Microanalyzer equipped with five wavelength-dispersive spectrometers. Electron microprobe analyses were conducted at 15 keV and 10 nA, with 10 s counting on peak elements and a beam size of 100 μm × 100 μm.

Electrical conductivity results. The dependence of electrical conductivity on temperature for each sample was fitted using an Arrhenius law

$$\sigma = \sigma_0 \times \exp[-E_a/(kT)]$$

with σ_0 being the pre-exponential factor (in units of S m^{-1}), E_a the activation energy (in electronvolts), k the Boltzmann constant (8.617×10^{-5} eV K^{-1}), and T the temperature (in kelvin). Values calculated for the pre-exponential factor and activation energy are presented in Extended Data Tables 3 and 4.

Electrical conductivity layered model. In this electrical model, the material considered alternating layers of sheared polycrystalline olivine and of olivine + 5 vol% MORB (layered model 1) or of basalt only (layered model 2). Electrical anisotropy can be modelled using series and parallel circuits, depending on the horizontal direction (x and y) of the electrical current. The vertical z direction is not considered since the magnetotelluric technique does not detect vertical anisotropy[35].

Series circuit. The direction of the electrical current is perpendicular to the shear plane. The equivalent resistance of the circuit, R_{eq}, corresponds to the sum of the resistances of each layer, R_i

$$R_{eq} = \sum_i R_i \quad (2)$$

The resistance R_i is calculated from values for σ from our study (sheared samples of polycrystalline olivine and of olivine + MORB) and from ref. 22 (basalt) using the relationship

$$R_i = \frac{1}{\sigma_i \times G_i} \quad (3)$$

with Gi the geometric factor of layer i (surface area divided by thickness). The bulk equivalent electrical conductivity is obtained using

$$\sigma_{eq} = \frac{1}{R_{eq} \times G} \quad (4)$$

where G is the geometric factor for the sample.

Application. We consider a cubic and layered material of size L = 1.5 mm (G = 1.5×10^{-3} m) made of five layers, two of olivine and three of olivine + MORB or of basalt. The dimensions of each olivine layer are 1.5 mm × 1.5 mm × 0.525 mm (geometric factor of 4.3×10^{-3} m), and the dimensions of each melt-bearing layer are 1.5 mm × 1.5 mm × 0.15 mm (geometric factor of 1.5×10^{-2} m). At 1,200 °C, the equivalent value of σ is 1.31×10^{-3} S m^{-1} (logσ = −2.88) for the material with basalt layers and 2.99×10^{-4} S m^{-1} (logσ = −3.52) for the material with 5 vol% MORB layers. At 1,300 °C, the equivalent value of σ is 2.13×10^{-3} S m^{-1} (logσ = −2.67) for the material with basalt layers and 1.08×10^{-3} S m^{-1} (logσ = −2.97) for the material with 5 vol% MORB layers.

Parallel circuit. In this case, the electrical current is parallel to the shear plane. The reciprocal of equivalent resistance equals the sum of the reciprocals of the resistance values

$$\frac{1}{R_{eq}} = \sum_i \frac{1}{R_i} \quad (5)$$

The resistance R_i is calculated from values of σ measured in our study (undeformed polycrystalline olivine and olivine + MORB) and reported in ref. 22 (for basalt).

The bulk equivalent electrical conductivity is obtained using the relationship

$$\sigma_{eq} = \frac{1}{R_{eq} \times G} \quad (6)$$

Application. We consider the same cubic material as above. With this direction for the current flow, the geometric factor of each olivine layer is 5.25×10^{-4} m and of each melt-bearing layer is 1.5×10^{-4} m. At 1,200 °C, the equivalent value of σ is 0.11 S m^{-1} (logσ = −0.96) for the material with basalt layers and 6.59×10^{-3} S m^{-1} (logσ = −2.18) for the material with 5 vol% MORB layers.

At 1,300 °C, the equivalent value of σ is 0.44 S m^{-1} ($\log\sigma = -0.36$) for the material with basalt layers and 1.40×10^{-2} S m^{-1} ($\log\sigma = -1.85$) for the material with 5 vol% MORB layers.

Electrical anisotropy. Electrical anisotropy is the ratio of electrical conductivity for the parallel circuits to electrical conductivity for the series circuits (that is, $\sigma_{\text{parallel circuit}}/\sigma_{\text{series circuit}}$). For the material containing 5 vol% MORB layers, electrical anisotropy is 22.0 (±2.0) and 13.0 (±0.1) at 1,200 °C and 1,300 °C, respectively. For the material containing basalt layers, higher values for electrical anisotropy of 82.9 (±7.5) and 207 (±29) at 1,200 °C and 1,300 °C, respectively, are obtained.

31. Stagno, V. & Frost, D. Carbon speciation in the asthenosphere: experimental measurements of the redox conditions at which carbonate-bearing melts coexist with graphite or diamond in peridotite assemblages. *Earth Planet. Sci. Lett.* **300,** 72–84 (2010).
32. King, D. S. H., Hier-Majumder, S. & Kohlstedt, D. L. An experimental study of the effects of surface tension in homogenizing perturbations in melt fraction. *Earth Planet. Sci. Lett.* **307,** 349–360 (2011).
33. Pommier, A. Leinenweber, K. & Tasaka, M. Experimental investigation of the electrical behavior of olivine during partial melting under pressure and application to the lunar mantle. *Earth Planet. Sci. Lett.* (in the press).
34. Ni, H., Keppler, H., Manthilake, M. A. & Katsura, T. Electrical conductivity of dry and hydrous $NaAlSi_3O_8$ glasses and liquids at high pressures. *Contrib. Mineral. Petrol.* **162,** 501–513 (2011).
35. Martí, A. The role of electrical anisotropy in magnetotelluric responses: from modelling and dimensionality analysis to inversion and interpretation. *Surv. Geophys.* **35,** 179–218 (2014).

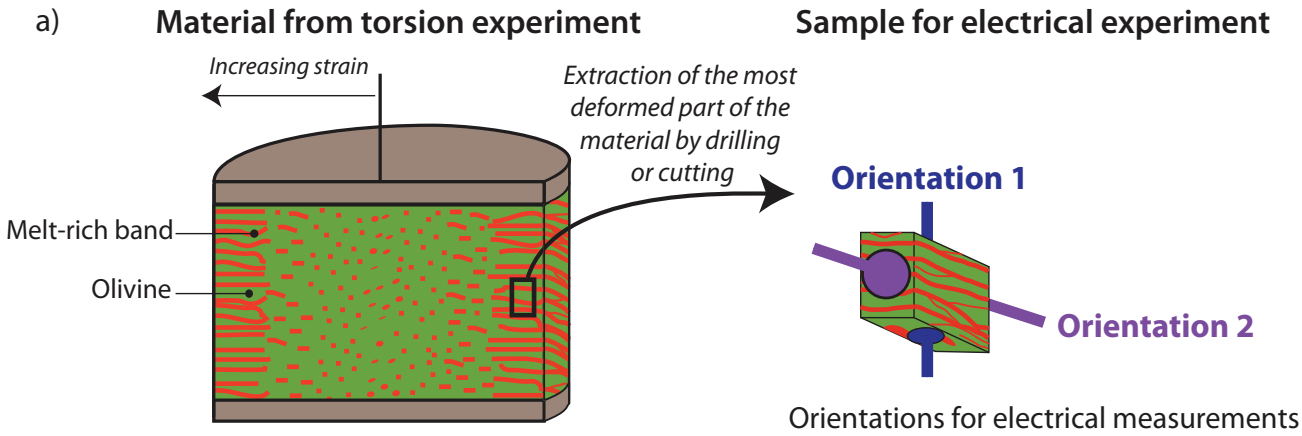

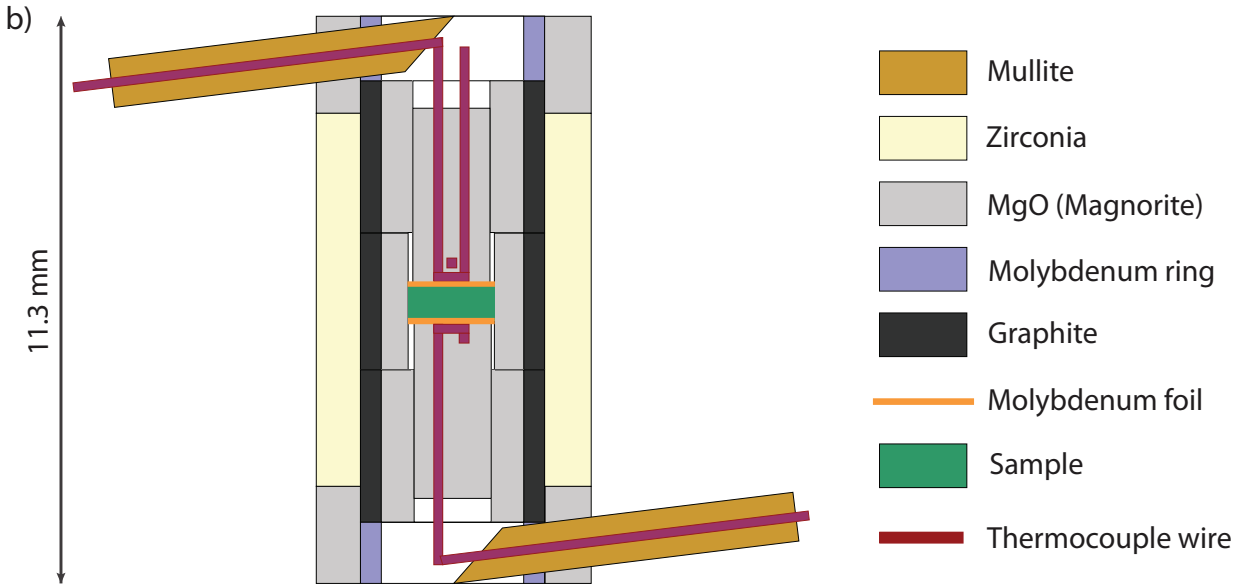

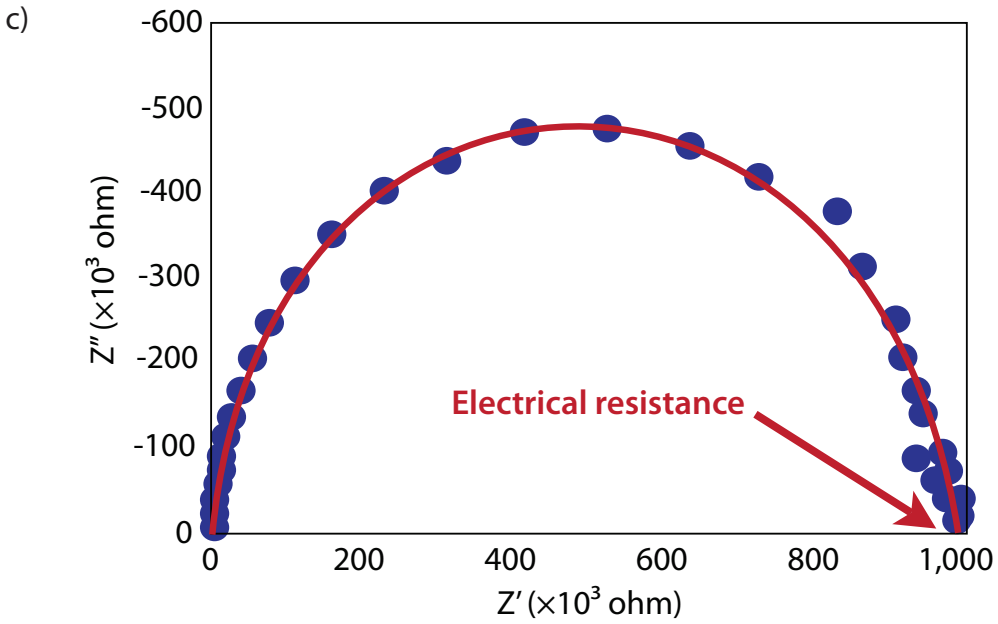

Extended Data Figure 1 | Experimental protocol. **a**, Starting material preparation. Deformed material is synthesized in a gas-medium apparatus at 300 MPa (left), and its outer part is extracted for electrical measurements in the multi-anvil apparatus at about 3 GPa (right). Two orientations of the sample are considered, leading to vertical (blue) and tangential (purple) electrical measurements. **b**, Cross-section of the electrical conductivity cell (14/8 multi-anvil assembly, that is, the corner-truncation edge length is 8 mm and the pressure media edge length is 14 mm). Both electrodes are made of W–Re thermocouple wire with one electrode also serving as a thermocouple. **c**, Example of a complex impedance spectrum (real part Z′ versus imaginary part Z′′) for a sheared sample of olivine + 5 vol% MORB sample at 750 °C and approximately 3 GPa. The intersection between the response of the sample (blue dots, each dot corresponding to one frequency) with the real axis corresponds to the electrical resistance of the sample. The corresponding electrical conductivity value is obtained using the geometric factor (the surface of the electrode divided by thickness of the sample).

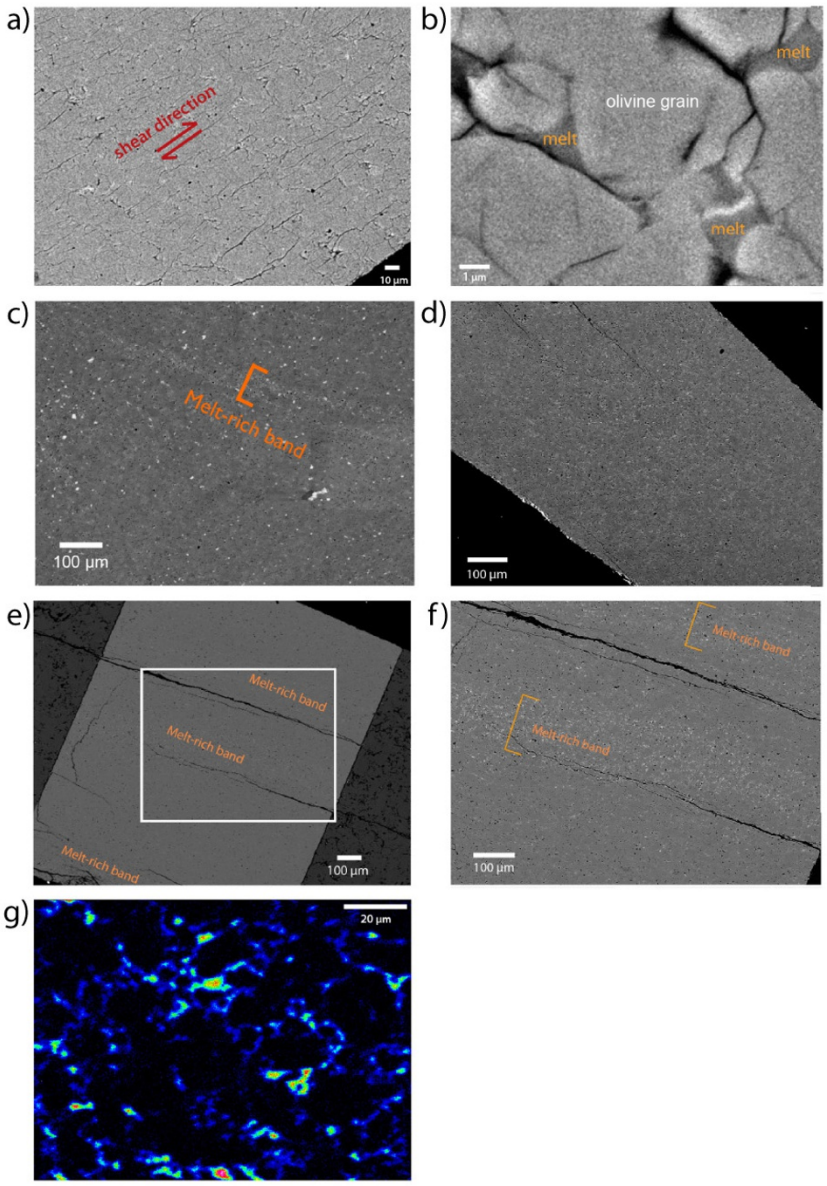

Extended Data Figure 2 | Texture and melt geometry. **a**, Back-scattered electron image of sheared sample PT0683-2 after electrical measurements, showing that deformation-induced melt texture was preserved during the experiment in the multi-anvil apparatus. **b**, Back-scattered electron image of sheared sample PT0756-2 after electrical measurements, illustrating the location of melt amongst the olivine grains. **c**, Starting material PT0683 showing the presence of melt-rich bands. **d**, Back-scattered electron image of sheared sample PT0683-1HT after electrical measurements at high temperature (up to 1,573 K). The absence of pronounced melt-rich bands suggests a loss in structural anisotropy, attributed to the effect of high temperature. These observations are consistent with electrical data that showed a noticeable decrease in electrical anisotropy with increasing temperature. **e**, Back-scattered electron image of sheared sample PT0683-1LT after electrical measurements at low temperature (<1,073 K), showing several light-coloured zones identified as melt-rich bands. The rectangle corresponds to the location of image **f** below. **f**, Zoom on melt-rich bands in sample PT0683-1LT. Melt is also present between the melt-rich zones as pockets amongst the olivine grains. **g**, Map of sodium distribution in sample PT0742-2 after electrical measurements. Colours correspond to the number of counts. Warm colours (reddish) correspond to high sodium concentration and are interpreted as pockets of carbonatite melt between olivine grains.

Extended Data Table 1 | Description of the starting materials.

Sample*	Composition	Av. grain size (micron)	Starting material synthesis						
			Deformation type	P (GPa)	T (K)	Stress (GPa)	Shear strain	Shear stress (GPa)	Shear strain rate (10^{-4} s^{-1})
Dry polycrystalline olivine									
PI1543-1	Fo_{90}	16	compression	0.3	1523	0.44	-	-	-
PI1543-2	Fo_{90}	16	compression	0.3	1523	0.44	-	-	-
PT0264-1	Fo_{90}	4-10	torsion	0.3	1473	-	3.5	0.24	3.5
PT0264-2	Fo_{90}	4-10	torsion	0.3	1473	-	3.5	0.24	3.5
Dry polycrystalline olivine + MORB									
PT0683-1LT	Fo_{90}+5% MORB	15	torsion	0.3	1473	-	1.2	0.12-0.15	4.6
PT0683-1HT	Fo_{90}+5% MORB	15	torsion	0.3	1473	-	1.2	0.12-0.15	4.6
PT0683-2	Fo_{90}+5% MORB	15	torsion	0.3	1473	-	1.2	0.12-0.15	4.6
PT0705-2	Fo_{90}+5% MORB	15	torsion	0.3	1473	-	9	0.12-0.15	1.5
PT0756-1	Fo_{90}+5% MORB	15	torsion	0.3	1473	-	2.16	0.12-0.15	5.5
PT0756-2	Fo_{90}+5% MORB	15	torsion	0.3	1473	-	2.16	0.12-0.15	5.5
Dry polycrystalline olivine + carbonate melt									
PT0742-1	Fo_{90}+2%$NaKCO_3$ melt	5-10	torsion	0.3	1473	-	3	0.12-0.15	1.1
PT0742-2	Fo_{90}+2%$NaKCO_3$ melt	5-10	torsion	0.3	1473	-	3	0.12-0.15	1.1
PT0742-3	Fo_{90}+2%$NaKCO_3$ melt	5-10	torsion	0.3	1473	-	3	0.12-0.15	1.1

* Extension: Electrical conductivity σ measurements perpendicular to deformation (-1), parallel to deformation (-2) and undeformed (centre of column) (-3), respectively. LT, low temperature; HT, high temperature.

Extended Data Table 2 | Electron microprobe analyses of most of the run products

Sample	Phase	SiO_2		TiO_2		Al_2O_3		Cr_2O_3		FeOtot		MnO		MgO		CaO		Na_2O		K_2O		NiO		Mg#	Sum
PT0683-1LT	ol(9)[a]	40.7	*(16)*[b]	-		-		-		10.4	*(11)*	0.11	*(2)*	48.8	*(32)*	-		-		-		0.35	*(3)*	*0.89*	100.5
	gl(1)	46.7		0.29		13.2		0.04		5.78		0.05		22.9		5.21		2.64		0.06		-		*0.88*	96.9
PT0683-2	gl(1)	47.0		0.22		16.0		0.01		5.23		0.05		22.9		6.26		2.24		0.12		-		*0.89*	99.9
PT0683-2bis	ol(17)	40.9	*(48)*							9.67	*(11)*	0.12	*(2)*	48.8	*(31)*	-		-		-		0.37	*(3)*	*0.90*	99.9
	gl(1)	47.4		1.62		12.6		0.02		6.82		0.11		21.4		7.1		2.15		0.15		-		*0.85*	99.3
PT0705-2	ol(17)	40.9	*(19)*	-		-		-		9.25	*(14)*	0.12	*(3)*	48.4	*(23)*	-		-		-		0.37	*(4)*	*0.90*	99.1
	gl(1)	45.7		0.34		13.4		0.02		5.03		0.17		26.7		5.42		1.85		0.07		-		*0.90*	98.7
PT0756-1	ol(12)	40.9	*(16)*	-		-		-		9.64	*(13)*	0.12	*(2)*	49.4	*(29)*	-		-		-		0.35	*(4)*	*0.90*	100.3
PT0756-2	ol(10)	41.0	*(29)*	-		-		-		10.0	*(19)*	0.14	*(2)*	48.0	*(34)*	-		-		-		0.37	*(2)*	*0.90*	99.5
	gl(3)	47.3	*(9)*	0.14	*(10)*	17.0	*(24)*	0.04	*(1)*	5.08	*(17)*	0.05	*(1)*	21.1	*(68)*	6.82	*(24)*	2.37	*(19)*	0.05	*(1)*	-		*0.88*	100.0
PT0742-1	ol(29)	41.0	*(15)*	-		-		-		8.44	*(47)*	0.12	*(3)*	50.5	*(36)*	-		-		-		0.36	*(4)*	*0.91*	100.3
PT0742-3	ol(10)	41.4	*(30)*	-		-		-		8.48	*(53)*	0.11	*(2)*	50.1	*(52)*	-		-		-		0.31	*(8)*	*0.91*	100.4

Contents are in weight per cent. Ol, olivine; gl, glass. A dash indicates 'not measured'. [a]The number of microprobe analyses is shown in parentheses. [b]One standard deviation in terms of least unit cited is shown in italics and parentheses; for example, 46.11(123) indicates a standard deviation of 1.23wt% on the value of 46.11wt%.

Extended Data Table 3 | Electrical results for polycrystalline olivine materials

Sample	Composition	Electrical conductivity experiments				Arrhenius equation parameters♦			
		P (GPa)	T (K)	Duration (hr)*	Rel. error on σ (%)	Ea (eV)	Error (eV)	Ln(σ_0), (σ_0 in S/m)	Error (S/m)
PI1543-1	Fo_{90}	2.8	1121-1575	2.0	7.5-10.5	0.959	0.005	0.56	0.003
PI1543-2	Fo_{90}	2.8	1274-1623	1.9	2.1-7.1	0.879	0.010	0.64	0.007
PT0264-1	Fo_{90}	2.8	873	0.5	2.2	-	-	-	-
PT0264-2	Fo_{90}	2.8	1173-1570	1.0	2.0-11.5	1.042	0.001	4.1	0.003

* Time spent in heating and cooling cycles.
♦ $\ln\sigma = \ln\sigma_0 - E_a/kT$.

Extended Data Table 4 | Electrical results for melt-bearing materials

Sample	Composition	Electrical conductivity experiments				Arrhenius equation parameters at T<~870°C ♦				Arrhenius equation parameters at T>~870°C ♦				Extrapolation of low-T data to T>Tg■		
		P (GPa)	T (K)	Duration (hr)*	Rel. error on σ (%)	Ea (eV)	Error (eV)	Ln(σ_0), (σ_0 in S/m)	Error (S/m)	Ea (eV)	Error (eV)	Ln(σ_0), (σ_0 in S/m)	Error (S/m)	Slope a	Intercept b	R^2
Dry polycrystalline olivine + MORB																
PT0683-1LT	Fo_{90}+5% MORB	2.8	847-1,073	1.0	0.8-1.6	1.047	0.030	3.5	0.100	-	-	-	-	-0.571	1.942	0.967
PT0683-1HT	Fo_{90}+5% MORB	2.8	1,395-1,466	1	4.1-5.1	-	-	-	-	1.223	0.047	6.0	0.667	-	-	-
PT0683-2	Fo_{90}+5% MORB	2.8	825-1,479	1.3	2.5-10.7	0.335	0.003	-3.6	0.028	0.691	0.010	0.14	0.002	-	-	-
PT0705-2	Fo_{90}+5% MORB	2.8	822-1,076	1.0	1.6-3.1	1.109	0.010	5.1	0.480	-	-	-	-	-0.542	2.023	0.984
PT0756-1	Fo_{90}+10% MORB	2.8	725-1,120	2.5	5.0-5.7	0.942	0.004	1.3	0.005	-	-	-	-	-0.499	0.775	0.995
PT0756-2	Fo_{90}+10% MORB	2.8	671-1,078	1.2	6.4-6.8	0.728	0.022	0.55	0.117	-	-	-	-	-0.178	-1.523	0.904
Dry polycrystalline olivine + carbonate melt																
PT0742-1	Fo_{90}+2% $NaKCO_3$ melt	2.8	1,023-1,473	2.0	1.6-4.2	0.381	0.018	-3.3	0.160	1.254	0.010	5.3	0.043	-	-	-
PT0742-3	Fo_{90}+2% $NaKCO_3$ melt	2.8	968-1,576	1.6	1.6-4.2	0.509	0.032	-3.1	0.196	1.358	0.013	5.6	0.053	-	-	-

* Time spent in heating and cooling cycles.

♦ $\ln\sigma = \ln\sigma_0 - E_a/kT$.

■ $\log\sigma_0 = a \times 10{,}000/T + b$.

Extended Data Table 5 | Uncertainties on electrical conductivity values for the experiment on sample PT0683-2

Temperature (K)	Resistance (ohm)	Electrical conductivity (S/m)	Error on conductivity (%)	Upper value (S/m)	Lower value (S/m)
825	1800000	0.00027	2.5	0.00028	0.00026
848	1680000	0.00029	2.5	0.00030	0.00028
878	1500000	0.00032	2.6	0.00034	0.00031
899	1320000	0.00037	2.8	0.00039	0.00035
922	1200000	0.00041	2.9	0.00043	0.00038
945	1100000	0.00044	3.0	0.00047	0.00042
975	1000000	0.00049	3.1	0.00052	0.00046
1001	860000	0.00057	3.4	0.00060	0.00053
1024	780000	0.00062	3.6	0.00067	0.00058
1050	700000	0.00070	3.8	0.00075	0.00064
1078	640000	0.00076	4.0	0.00082	0.00070
1098	590000	0.00083	3.3	0.00088	0.00077
1126	520000	0.00094	3.6	0.00100	0.00087
1144	480000	0.00101	3.7	0.00109	0.00094
1176	420000	0.00116	4.0	0.00125	0.00107
1196	360000	0.00135	4.4	0.00147	0.00123
1221	294000	0.00166	5.0	0.00182	0.00149
1245	260000	0.00187	5.5	0.00208	0.00167
1277	220000	0.00221	6.2	0.00249	0.00194
1321	172000	0.00283	7.5	0.00325	0.00241
1378	136000	0.00358	9.0	0.00423	0.00294
1422	116000	0.00420	10.3	0.00506	0.00334
1479	110000	0.00443	10.7	0.00538	0.00348